MATERIALS CHEMISTRY FRONTIERS

CCS 中国化学会 CHINESE CHEMICAL SOCIETY

ICCAS

ROYAL SOCIETY OF CHEMISTRY

RESEARCH ARTICLE

View Article Online
View Journal | View Issue

Cite this: *Mater. Chem. Front.*, 2020, **4**, 3539

Perylene monoimide and naphthalene-annulated [3,3,3]propellanes: synthesis and device applications†

Lingling Lv,[a] Wenda Sun,[b] Zhenmei Jia,[a] Guowei Zhang,[a] Fuzhi Wang,[b] Zhan'ao Tan *[ab] and Lei Zhang *[a]

Received 29th October 2019,
Accepted 27th November 2019

DOI: 10.1039/c9qm00668k

rsc.li/frontiers-materials

Rigid three-dimensional polycyclic aromatic hydrocarbons (3D PAHs) are garnering great interest due to their unique molecular shapes and interesting optoelectronic properties. Herein we report the synthesis of two 3D PAHs with perylene monoimide (PMI) and naphthalene subunits fused on [3,3,3]propellanes. The resulting compounds (**P-1** and **P-2**) are unambiguously characterized by spectral analysis and theoretical calculations. It is found that the subunits can significantly influence the electronic properties and electron communications in 3D PAHs. In contrast to the naphthalene subunit, the PMI subunit leads to the enhancement of electron communication in 3D PAHs and amplifies the absorption coefficients when compared to the individual PMI subunit. In addition, UV-vis measurement suggests the presence of homoconjugation between the subunits. These compounds exhibit p-type behaviors with the mobilities on the order of 10^{-5} to 10^{-4} cm^2 V^{-1} s^{-1}. Additionally, these 3D PAHs show strong fluorescence and are employed as emitters for organic light-emitting diodes.

1. Introduction

In recent years, there has been growing interest in the synthesis of rigid three-dimensional polycyclic aromatic hydrocarbons (3D PAHs) by fusion of five- or six-membered aromatic rings to 3D scaffolds.[1] These rigid structures are critical to advances in a number of research areas and appear as attractive candidates for gas diffusion, sensory response, and super molecular assemblies.[2] Among the multiple applications, their use in organic semiconductors is particularly promising.[3] In principle, 3D PAHs possess a degree of rigidity and conjugation in three directions, which provides the potential options to tune the through-space interactions between PAH units and of self-assembly in the solid state that have significant effects on the electronic properties, stability, solubility and device performance.[4] Therefore, this leads to a large number of applications ranging from light emitting diodes (LEDs), to energy storage systems, organic field-effect transistors (OFETs), and organic photovoltaics (OPVs). For instance, Mastalerz *et al.* synthesized two triptycene-based aroylenimidazoles, which acted as potential non-fullerene acceptor materials in bulk heterojunction organic solar cells.[5] Another example was from the Wang group, who synthesized a series of π-extended triptycenes fused with perylene diimides (PDIs) as a non-fullerene acceptor for organic solar cells.[6] Furthermore, Nuckolls *et al.* reported a promising class of 3D nanographenes based on triptycene, which were used as electron-extracting layers to decrease contact resistances in perovskite solar cells and led to power conversion efficiencies greater than 18%.[7] Additionally, Bunz *et al.* demonstrated that triptycene-based azaacenes show promising OLED performance due to their highly fluorescent amorphous character.[8]

To fully realize the potential of 3D PAHs as candidates for promising optoelectronic materials, it is critical to develop synthetic methods for 3D scaffolds, as well as their incorporation into more complex, extended π-systems.[9] However synthetic access to these 3D scaffolds and their extended π-systems remains a great challenge owing to the generally considerable strains involved. Although triptycene has been extensively used during the past two decades to prepare extended 3D PAHs by lateral fusion of aromatic rings to the benzene rings, up to now, the number of 3D scaffolds and complex 3D PAHs are still very rare.[10] Recently, Kubo *et al.* demonstrated that trinaphtho[3.3.3]propellane (TNP) is another highly versatile building block for the construction of large 3D PAHs.[11] With its three naphthalene units, this propellane has the ability to use well-established synthetic chemistry to prepare large and complex 3D PAHs. For example, Kubo *et al.*

[a] *Beijing Advanced Innovation Center for Soft Matter Science and Engineering, Beijing University of Chemical Technology, Beijing 100029, P. R. China. E-mail: zhl@mail.buct.edu.cn, tanzhanao@mail.buct.edu.cn*

[b] *State Key Laboratory of Alternate Electrical Power System with Renewable Energy Sources, North China Electric Power University, Beijing 102206, P. R. China*

† Electronic supplementary information (ESI) available: ^{1}H NMR, ^{13}C NMR, and HRMS of the compounds, theoretical calculations, device fabrication and characterization. See DOI: 10.1039/c9qm00668k

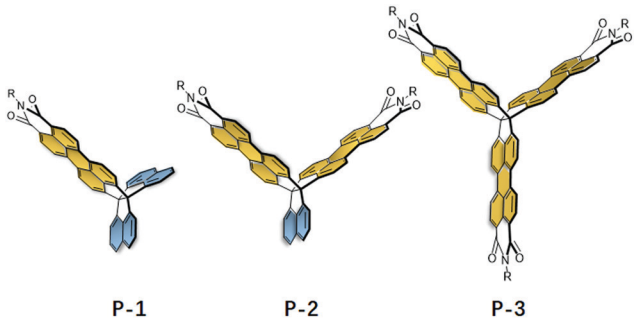

Fig. 1 Chemical structures of **P-1**, **P-2**, and **P-3**.

successfully prepared π-extended TNPs using palladium-catalyzed cross-coupling reactions, which co-crystallized with the acceptor, leading to the formation of 2D honeycomb lattices.[12] Inspired by these works, we recently reported a novel 3D-symmetric scaffold, triperyleno[3,3,3]propellane triimides (**P-3**) (Fig. 1), that possesses three perylene monoimide subunits fused on a propellane.[13] This scaffold is compatible with different reactions to readily prepare quasi-D_{3h} symmetric nanostructures that show isotropic charge transport despite the weak intermolecular interactions between the neighboring PAH units.

Herein, we report the synthesis and characterization of trinaphtho[3.3.3]propellanes in which either one (**P-1**) or two (**P-2**) naphthalene units are replaced by perylene monoimide (PMI) units. We envision that the resulting 3D structures could provide key differences in electronic structure, stability, aggregation and device performance, which could provide deep understanding of the structure–property relationships in 3D PAHs. We discuss in detail the synthetic approaches, electronic structures, and organic device performance of **P-1**, **P-2**, and **P-3** by using combined experimental and theoretical approaches. In addition, with PMI and naphthalene units, the resulting **P-1** and **P-2** can be regarded as two new 3D scaffolds to prepare large complex 3D PAHs.

2. Results and discussion

Synthesis

Scheme 1 shows the synthesis of **P-1** and **P-2**. Bromination of trinaphtho[3.3.3]propellane (TNP, **1**) with Br_2 provided monobrominated **2** in 72% yield and dibrominated **3** in 53% yield, which were then readily converted to the corresponding borates **4** and **5** in moderate yields. The subsequent Suzuki coupling reactions between 4-bromonaphthalic anhydride with the borates provided **6** and **7**, which was followed by ring closure with $AlCl_3$ as an oxidant to afford the desired dicarboxylic anhydrides **8** in 45% yield and **9** in 35% yield. Finally, compounds **8** and **9** were converted into **P-1** in 78% yield and **P-2** in 65% yield *via* the imidization reaction with an amine in N,N-dimethylformamide (DMF). The resulting **P-1** and **P-2** are soluble in common solvents and unambiguously verified by spectroscopic analysis.

Electronic structures, and optical, and redox properties

Fig. 2A shows the UV-vis absorption spectra of PMI, **P-1**, **P-2**, and **P-3** in chloroform. The absorption maximum of **P-1** (538 nm) is red-shifted by 32 nm relative to PMI (506 nm), which indicates the presence of intramolecular homoconjugation between the PMI and naphthalene units. When moving from **P-1** to **P-2**, there is a red-shift of 17 nm due to the extended

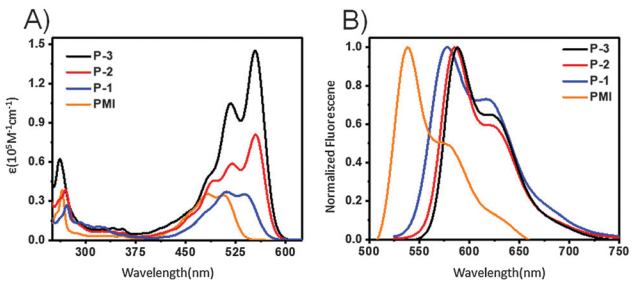

Fig. 2 (A) UV/vis absorption and (B) photoluminescence spectra of PMI, **P-1**, **P-2**, and **P-3** in chloroform (~10^{-5} M).

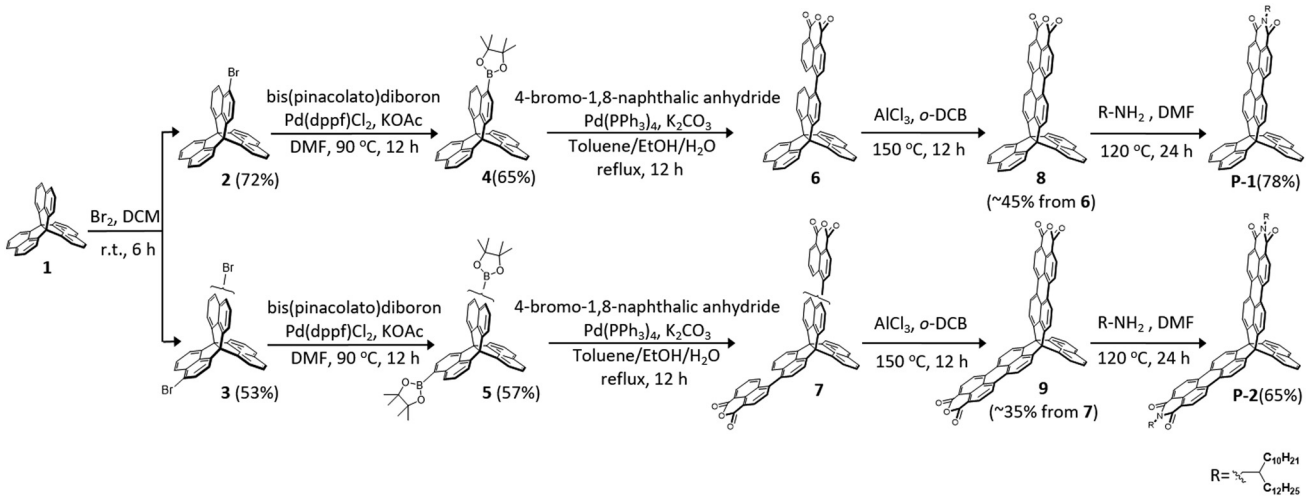

Scheme 1 Synthetic steps to **P-1** and **P-2**.

conjugation of the subunit. However, we observe that from **P-2** to **P-3**, the absorption maximum appears to behave independently with conjugation of the subunit, but exhibits different absorption coefficients. For compound **P-1**, the maximum absorption coefficient is 34 800 M^{-1} cm^{-1}, which is almost identical to that of PMI (34 100 M^{-1} cm^{-1}). However, the maximum absorption coefficient of **P-2** is 80 700 M^{-1} cm^{-1}, which is significantly larger than the sum of the two PMI units ($2 \times 34\,100$ M^{-1} cm^{-1} = 68 200 M^{-1} cm^{-1}). The similar amplification of the maximum absorption coefficient (151 700 M^{-1} cm^{-1}) of **P-3** is also found in contrast to the sum of the three PMI units (151 700 $>$ $3 \times 34\,100$ M^{-1} cm^{-1}). As shown in Fig. 2B, compounds **P-1**, **P-2**, and **P-3** show strong emission bands at 579, 585, and 588 nm, with florescence quantum yields of 83.0, 88.8 and 85.3%, respectively. Additionally, the optical band gaps estimated from the absorption edges are 2.16 and 2.13 eV for **P-1** and **P-2**, respectively. Time-dependent density functional theory (TD-DFT) calculations at the B3LYP/6-31G(d,p) level of theory were performed to better understand the nature of the molecular excited-state characteristics. According to the calculations, the lowest lying excitations for **P-1** and **P-2** are attributed to the HOMO to LUMO transitions. The calculated maximum absorptions for **P-1** and **P-2** are estimated to be 512 nm (f_{calc} = 0.65) and 563 nm (f_{calc} = 0.68), which are in good agreement with the experimental absorption values (Table 1).

The redox properties of **P-1** and **P-2** were examined by electrochemical experiments (0.1 M $TBAPF_6$, 100 mV s^{-1}) in dichloromethane and the onset oxidation–reduction potentials were determined relative to Fc/Fc^+ (4.8 eV) (Fig. 3A). The CVs of PMI and **P-1** exhibit two reversible reduction peaks and one reversible oxidation peak, respectively. The first-wave reduction potential of **P-1** is −1.40 V, which is slightly more positive than those of PMI (−1.45 V). In contrast to the CV of **P-1** exhibiting two reduction waves and an oxidation wave, the CV of **P-2** reveals a splitting into three reduction waves and two oxidation waves and the CV of **P-3** shows four reduction waves and three oxidation waves. The splitting is attributed to the coulombic repulsion from the electrons in neighboring PMI subunits, which indicates electronic communication between different PMI subunits, whereas their first-wave oxidation and reduction potentials of **P-2** and **P-3** are essentially comparable with those of **P-1**, which indicates that there are no significant conjugative interactions between the individual PMI units. According to their onset potentials, the LUMO/HOMO values of **P-1**, **P-2**, and **P-3** are estimated to be −3.40/−5.71, −3.41/−5.71, and −3.38/−5.68 eV, respectively (relative to Fc/Fc+, 4.8 eV). DFT calculations reveal that the calculated HOMO and LUMO of **P-1** are mainly localized on the PMI unit. For **P-2**, the HOMO and LUMO are mainly localized on the two PMI units (Fig. 3B). For **P-3**, the HOMO is delocalized across the three PMI units and the LUMO is delocalized on only two PMI units.[13]

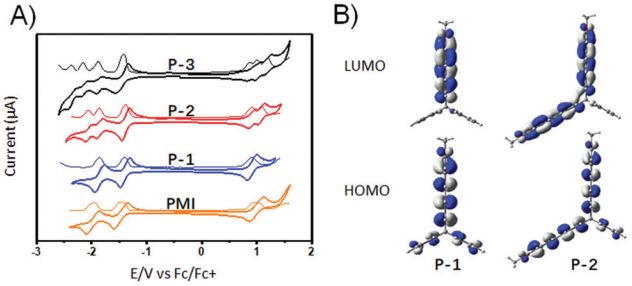

Fig. 3 (A) Cyclic voltammograms (bold solid lines) and differential pulse voltammograms (thin solid lines) of **P-3**, **P-2**, **P-1**, and PMI. All experiments were performed in nitrogen-purged dichloromethane with tetrabutylammonium hexafluorophosphate (TBAPF6, 0.1 M) as the supporting electrolyte with a scan of 100 mV s^{-1}. (B) Molecular orbitals (HOMO and LUMO) of **P-1** and **P-2** obtained from B3LYP/6-31G(d,p) calculation (alkyl chains are replaced by methyl groups).

Semiconductor properties

We further explored the charge-carrier transport properties of the 3D materials. Thin-film OFETs of **P-1**, **P-2**, and **P-3** were fabricated in the "bottom-gate bottom-contact" geometry by spin-coating a chloroform solution onto OTS-SiO_2/Si substrates. The films showed p-type charge-carrier transport characteristics under nitrogen. Although these compounds have strong electron-deficient imide groups, no electron transport is observed. We surmise that this is due to large injection barriers for electrons in this device configuration. For **P-1** and **P-2**, the devices showed mobilities of 2.2×10^{-4} and 3.5×10^{-4} cm^2 V^{-1} s^{-1}, respectively, whereas the **P-3** device showed mobility of 2.5×10^{-5} cm^2 V^{-1} s^{-1} (Fig. 4). The relatively low mobility of **P-3** could be a result of low crystallinity in the thin film, as evident from AFM images that show an RMS of 0.37 nm (Fig. S2, ESI†).

Due to the strong fluorescence, these 3D PAHs were employed as emitters for organic light-emitting diodes. The device structure and the energy level diagram are shown in Fig. 5A and B.

Table 1 Photophysical properties and electrochemical data for PMI, **P-1**, **P-2**, and **P-3**

	Uv-vis[a]				CV[c]					
	λ_{max} (nm)	ε_{max} (M^{-1} cm^{-1})	λ_{emi} (nm)	Φ_{fl}[b] (%)	$E_{1/2}^{red}$ (V)	$E_{1/2}^{ox}$ (V)	LUMO (eV)	HOMO (eV)	E_g^{cv} (eV)	E_g^{opt} (eV)
P-3	555	151 694	588	85.3	−1.42	0.88	−3.38	−5.68	2.30	2.13
P-2	555	80 741	585	88.8	−1.39	0.91	−3.41	−5.71	2.30	2.13
P-1	538	34 836	579	83.0	−1.40	0.91	−3.40	−5.71	2.31	2.16
PMI	506	34 100	538	92.0	−1.45	1.00	−3.35	−5.80	2.45	2.33

[a] The photophysical properties of the compounds were measured in $CHCl_3$ (10^{-5} M). [b] Measured in dilute $CHCl_3$ solution (10^{-5} M) and calculated by the absolute quantum yield method. [c] CVs were measured in dichloromethane with tetrabutylammonium hexafluorophosphate ($TBAPF_6$, 0.1 M) as the supporting electrolyte with a scan of 100 mV s^{-1}; $E_{1/2}^{ox}$ and $E_{1/2}^{red}$ are half-wave potentials of the first oxidative and reductive waves (*vs.* Fc/Fc^+); the LUMO and HOMO values were calculated from the onset of the first reduction and oxidation peaks, respectively; E_g^{cv} is the electrochemical HOMO–LUMO gap; E_g^{opt} is the optical band gap and estimated from the onset of the absorption peak.

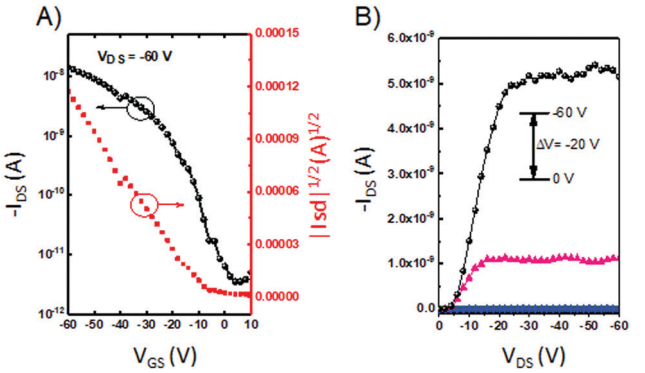

Fig. 4 (A) Transfer and (B) output curves based on a thin film transistor of **P-3** annealed at 160 °C.

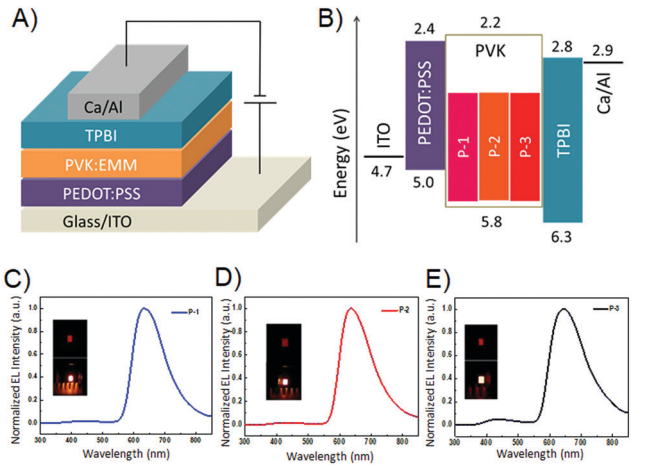

Fig. 5 LED structure, energy diagram and electroluminescence (EL) spectra. (A) The device structure and (B) flat-band energy level diagram of a conventional LED. The normalized EL spectra of (C) **P-1**, (D) **P-2** and (E) **P-3** as emitting materials (insets are the pictures of the LED).

Patterned indium tin oxide (ITO) is used as an anode with a 30 nm layer of poly(3,4-ethylenedioxythiophene):poly-(styrenesulfonate) (PEDOT:PSS) as a hole injection layer. The cathode is composed of 20 nm Ca and 80 nm Al. Poly(*N*-vinyl carbazole) (PVK) is used as a host material due to its good film forming and hole transporting properties and its wide band gap is beneficial to avoid parasitic emission.[14] A 40 nm layer 1,3,5-tris(*N*-phenylbenzimidazol-2-yl) benzene (TPBI) is used as the electron transporting layer. **P-1**, **P-2**, and **P-3** are used as guest emitters with the thickness of 40 nm. Red emission from **P-1**, **P-2**, and **P-3** can be observed for the OLEDs under forward bias, and the EL spectra are shown in Fig. 5C–E. Their emission peaks are located at 632, 636, and 643 nm, respectively. The electroluminescence performance of the devices is shown in Fig. 6, and the corresponding parameters are listed in Table 2. As shown in Fig. 6A, the three devices show obvious differences in current density, which can be ascribed to their different molecular structures. **P-1** has the highest current density, while **P-3** has the lowest current density. As can be seen from Fig. 6B, the devices using **P-1** and **P-2** as emitting materials show similar turn-on voltage of around 4.1 V. However, the turn-on voltage of **P-3** is relatively high, reaching 6.5 V. The maximum brightness of **P-1**-LED reaches 1856 cd m^{-2}. It can be seen from Fig. 6C that the current efficiencies of **P-1** and **P-2** can reach 1.0 cd A^{-1}.

Table 2 Parameters of LEDs with different emitting materials

LED	V_{on} (V)	L_{max} (cd m^{-2})	η (cd A^{-1})	PL_{max}	EL_{max} (nm)
P-1	4.1	1856	1.14	579	632
P-2	4.1	1400	1.09	585	636
P-3	6.5	963	0.42	588	643

3. Conclusions

In summary, we have described the synthesis and characterization of new 3D PAHs with PMI and naphthalene as subunits. The comparative study of **P-1**, **P-2**, and **P-3** indicates that the subunit plays an important role in the optical properties and electron communication between subunits. Compared to that of **P-1**, the longest absorptions of **P-2** and **P-3** are red-shifted by 17 nm. The amplification of the absorption coefficients of **P-2** and **P-3** are observed when compared to that of the PMI unit. Electrochemical experiments reveal that the weak interactions between the PMI units of **P-2** and **P-3** lead to multiple redox states. **P-1**, **P-2**, and **P-3** show p-type behaviors with the mobilities on the order of 10^{-5} to 10^{-4} cm^2 V^{-1} s^{-1}. In particular, these 3D

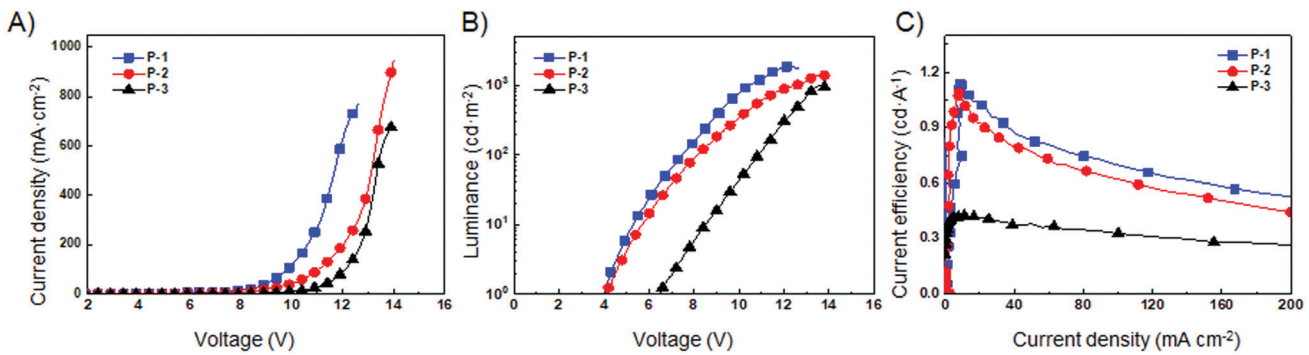

Fig. 6 Electroluminescence performance of different LEDs. (A) Current density–voltage (*J*–*V*), (B) luminance–voltage (*L*–*V*) and (C) current efficiency–current density (η–*J*) curves.

PAHs serve as emitters for organic light-emitting diodes due to strong fluorescence. We are currently exploring the use of these 3D PAHs as building blocks to prepare even larger, more complex 3D propellanes for organic devices.

4. Experimental section

Synthesis

All chemical reagents were purchased from commercial suppliers and used without further purification unless otherwise specified. THF was freshly distilled prior to use.

Synthesis of 2

To a solution of trinaphtho[3.3.3]propellane (2 g, 4.98 mmol) in dichloromethane (50 ml) was added elemental bromine (0.88 g, 5.47 mmol) and the solution was stirred at room temperature for 6 h. After quenching with saturated aqueous sodium sulfite, the aqueous layer was extracted with dichloromethane. The combined organic layer was washed with brine and then dried over anhydrous sodium sulfate. After the solvent was removed by vacuum, the resulting residue was purified using a silica gel column with petroleum ether/dichloromethane (3 : 1 to 4 : 1, v/v) to give compound **2** (1.72 g, 72% yield) as a brown powder. ^{1}H NMR (400 MHz, $CDCl_3$, 300 K) δ = 8.09 (d, J = 7.1 Hz, 1H), 8.06–7.98 (m, 4H), 7.90 (d, J = 7.5 Hz, 1H), 7.80 (dd, J = 12.6, 8.0 Hz, 2H), 7.68–7.52 (m, 9H); ^{13}C NMR (101 MHz, $CDCl_3$, 300 K) δ = 146.69, 146.32, 146.20, 138.21, 137.24, 132.60, 131.82, 129.96, 128.71, 124.56, 124.54, 123.92, 120.35, 120.08, 119.34, 119.28, 119.17, 80.16, 79.34; HR-MALDI-TOF (m/z): calcd for $C_{32}H_{17}Br$: 480.0508; found 480.0510.

Synthesis of 3. To a solution of trinaphtho[3.3.3]propellane (1.6 g, 3.85 mmol) in dichloromethane (45 ml) was added elemental bromine (1.28 g, 7.96 mmol) and the solution was stirred at room temperature for 6 h. After quenching with saturated aqueous sodium sulfite, the aqueous layer was extracted with dichloromethane. The combined organic layer was washed with brine and then dried over anhydrous sodium sulfate. After the solvent was removed by vacuum, the resulting residue was purified using a silica gel column with petroleum ether/dichloromethane (4 : 1 to 7 : 1, v/v) to give compound **3** as a brown solid (1.47 g, 53% yield). ^{1}H NMR (400 MHz, $CDCl_3$, 300 K) δ = 8.09–7.97 (m, 4H), 7.90–7.76 (m, 6H), 7.68–7.60 (m, 4H), 7.55 (t, J = 7.5 Hz, 2H); ^{13}C NMR (101 MHz, $CDCl_3$, 300 K) δ = 146.64, 146.52, 146.21, 146.10, 145.87, 145.75, 145.64, 138.11, 137.14, 132.60, 131.87, 131.85, 130.00, 128.76, 124.75, 124.73, 124.71, 124.12, 124.10, 120.37, 120.32, 120.10, 120.04, 119.37, 119.35, 119.31, 119.25, 80.24, 79.43, 78.62; HR-MALDI-TOF (m/z): calcd for $C_{32}H_{16}Br_2$: 557.9613; found 557.9617.

Synthesis of 4. Compound **2** (2.32 g, 4.82 mmol) and bis-(pinacolato)diboron (1.47 g, 5.78 mmol) were dissolved in anhydrous DMF (50 ml) in a two-neck round bottomed flask. Potassium acetate (1.42 g, 14.46 mmol) and Pd(dppf)Cl_2 (0.18 g, 0.24 mmol) were then quickly added into the flask. The resulting mixture was vigorously stirred under nitrogen and heated at 90 °C for 24 hours. After cooling, the precipitate was washed with methanol and purified by column chromatography on silica gel, and eluted with petroleum ether/dichloromethane (1 : 1 to 1 : 2 v/v) to give compound **4** (1.62 g, 65% yield) as a white powder. ^{1}H NMR (400 MHz, $C_2D_2Cl_4$, 373 K) δ = 8.48 (d, J = 8.4 Hz, 1H), 8.20 (d, J = 7.1 Hz, 1H), 8.07 (t, J = 7.4 Hz, 6H), 7.69–7.57 (m, 9H), 1.36 (s, 12H); ^{13}C NMR (101 MHz, $C_2D_2Cl_4$, 373 K) δ = 150.75, 147.44, 147.39, 147.09, 138.99, 137.99, 137.43, 136.99, 133.21, 129.67, 129.33, 126.72, 125.06, 124.98, 120.04, 120.00, 119.94, 119.51, 84.36, 80.47, 80.34, 25.69; HR-MALDI-TOF (m/z): calcd for $C_{38}H_{29}BO_2$: 528.2261; found 528.2252.

Synthesis of 5. Compound **3** (2.60 g, 4.66 mmol) and bis-(pinacolato)diboron (2.84 g, 11.18 mmol) were dissolved in anhydrous DMF (55 ml) in a two-neck round bottomed flask. Potassium acetate (2.74 g, 27.96 mmol) and Pd(dppf)Cl_2 (0.17 g, 0.23 mmol) were then quickly added into the flask. The resulting mixture was vigorously stirred under nitrogen and heated at 90 °C for 24 hours. After cooling, the precipitate was washed with methanol and purified by column chromatography on silica gel, and eluted with petroleum ether/dichloromethane (1 : 1 to 1 : 2 v/v) to give compound **5** as a white solid (1.74 g, 57% yield). ^{1}H NMR (400 MHz, $C_2D_2Cl_4$, 373 K) δ = 8.45 (d, J = 8.4 Hz, 2H), 8.18 (d, J = 7.1 Hz, 2H), 8.05 (dd, J = 12.0, 5.1 Hz, 6H), 7.66–7.55 (m, 6H), 1.35 (s, 24H); ^{13}C NMR (101 MHz, $C_2D_2Cl_4$, 373 K) δ = 150.80, 147.17, 138.95, 138.01, 137.46, 137.01, 133.21, 129.63, 129.32, 129.28, 126.75, 125.01, 120.01, 119.95, 119.48, 84.34, 80.10, 25.69; HR-MALDI-TOF (m/z): calcd for $C_{44}H_{40}B_2O_4$: 654.3122; found 654.3116.

Synthesis of 6. A two-necked flask was charged with a mixture of compound **4** (1 g, 1.89 mmol), 4-bromo-1,8-naphthalic anhydride (0.63 g, 2.27 mmol), Pd(PPh_3)$_4$ (0.11 g, 0.10 mmol), EtOH (18 ml), and 2 M Na_2CO_3 (6 ml) in toluene (120 ml) under argon, then warmed up to 85 °C with vigorous stirring overnight. After cooling to room temperature, the resulting white precipitate was collected by vacuum filtration and then washed with methanol, and acetone to give compound **6** (1.01 g, 90% yield) as a white powder. The obtained crude product was used in the next step without further purification. HR-MALDI-TOF (m/z): calcd for $C_{44}H_{22}O_3$: 598.1574; found 598.1577.

Synthesis of 7. A two-necked flask was charged with a mixture of compound **5** (1.5 g, 2.30 mmol), 4-bromo-1,8-naphthalic anhydride (1.40 g, 5.04 mmol), Pd(PPh_3)$_4$ (0.14 g, 0.12 mmol), EtOH (27 ml), and 2 M Na_2CO_3 (9 ml) in toluene (180 ml) under argon, then warmed up to 85 °C with vigorous stirring overnight. After cooling to room temperature, the resulting white precipitate was collected by vacuum filtration and then washed with methanol, and acetone to give compound **7** as a white solid (1.64 g, 85% yield). The obtained crude product was used in the next step without further purification. HR-MALDI-TOF (m/z): calcd for $C_{56}H_{26}O_6$: 794.1735; found 794.1737.

Synthesis of 8. To a solution of compound **6** (0.92 g, 1.54 mmol) in *o*-dichlorobenzene (50 ml), $AlCl_3$ (2 g, 15.0 mmol) was added. The resulting mixture was heated to 150 °C for 12 hours under nitrogen. After cooling, the resulting solution was added to 2 M HCl (200 ml) and stirred for another 2 h. The crude product was filtrated and washed with methanol and hot THF to give compound 8 (45% from 4) as a black red solid.

HR-MALDI-TOF (*m*/*z*): calcd for $C_{44}H_{20}O_3$: 596.1407; found 596.1407.

Synthesis of 9. To a solution of compound **7** (1.4 g, 1.76 mmol) in *o*-dichlorobenzene (60 ml), $AlCl_3$ (2.35 g, 17.60 mmol) was added. The resulting mixture was heated to 150 °C for 12 hours under nitrogen. After cooling, the resulting solution was added to 2 M HCl (200 ml) and stirred for another 2 h. The crude product was filtrated and washed with methanol and hot THF to give compound **9** as a black red solid (35% from **5**). HR-MALDI-TOF (*m*/*z*): calcd for $C_{56}H_{22}O_6$: 790.1422; found 790.1428.

Synthesis of P-1. In a two neck round-bottomed flask, a mixture of compound **8** (0.3 g, 0.50 mmol) and 2-decyl-1-tetradecanamine (0.89 g, 2.52 mmol) was dissolved in anhydrous DMF (50 ml). The reaction mixture was deoxygenated and heated to 120 °C for 24 hours. After cooling, the reaction mixture was poured into water and stirred for another 2 h, and then extracted with dichloromethane and dried by anhydrous Na_2SO_4. After the solvent was removed by vacuum, the resulting residue was purified using a silica gel column with petroleum ether/dichloromethane (1 : 1, v/v) to give compound **P-1** (0.37 g, 78% yield) as a red solid. ^{1}H NMR (500 MHz, $C_2D_2Cl_4$, 373 K) δ = 8.51 (d, J = 8.0 Hz, 2H), 8.18 (d, J = 7.7 Hz, 2H), 8.11 (d, J = 7.1 Hz, 6H), 8.05 (d, J = 7.6 Hz, 2H), 7.74 (d, J = 8.1 Hz, 4H), 7.69–7.65 (m, 4H), 4.18 (d, J = 7.2 Hz, 2H), 2.13–2.09 (m, 1H), 1.30 (d, J = 17.1 Hz, 40H), 0.90 (q, J = 7.0 Hz, 6H);^{13}C NMR (126 MHz, $C_2D_2Cl_4$, 373 K) δ = 164.92, 149.73, 146.26, 138.59, 137.96, 137.28, 133.46, 132.13, 131.03, 129.50, 128.54, 128.15, 127.77, 126.06, 125.52, 122.00, 121.75, 120.50, 120.21, 81.27, 45.62, 37.57, 32.95, 32.61, 30.85, 30.37, 30.33, 29.99, 27.46, 23.32, 14.69; HR-MALDI-TOF (*m*/*z*): calcd for $C_{68}H_{69}NO_2$: 931.5334; found 931.5338.

Synthesis of P-2. In a two neck round-bottomed flask, a mixture of compound **9** (0.42 g, 0.54 mmol) and 2-decyl-1-tetradecanamine (0.95 g, 2.68 mmol) was dissolved in anhydrous DMF (50 ml). The reaction mixture was deoxygenated and heated to 120 °C for 24 hours. After cooling, the reaction mixture was poured into water and stirred for another 2 h, then extracted with dichloromethane and dried by anhydrous Na_2SO_4. After the solvent was removed by vacuum, the resulting residue was purified by silica gel column with petroleum ether/dichloromethane (1 : 1, v/v) to give compound **P-2** as a red solid (0.50 g, 65% yield). ^{1}H NMR (500 MHz, $C_2D_2Cl_4$, 373 K) δ = 8.58 (d, J = 7.8 Hz, 4H), 8.43 (d, J = 7.4 Hz, 4H), 8.30 (d, J = 7.8 Hz, 4H), 8.20 (d, J = 7.5 Hz, 4H), 8.16 (d, J = 7.0 Hz, 2H), 7.80 (d, J = 8.1 Hz, 2H), 7.72 (t, J = 7.5 Hz, 2H), 4.16 (d, J = 6.8 Hz, 4H), 2.09 (s, 2H), 1.27 (s, 80H), 0.91–0.86 (m, 12H).;^{13}C NMR (126 MHz, $C_2D_2Cl_4$, 373 K) δ = 164.84, 148.49, 145.19, 138.63, 137.13, 133.60, 132.18, 131.07, 129.66, 129.41, 129.13, 128.21, 128.03, 126.15, 125.95, 122.33, 121.90, 120.76, 120.37, 81.08, 45.64, 37.57, 32.93, 32.60, 30.82, 30.36, 30.31, 29.98, 27.43, 23.31, 14.67; HR-MALDI-TOF (*m*/*z*): calcd for $C_{104}H_{120}N_2O_4$: 1460.9248; found 1460.9254.

Synthesis of P-3. Compound **P-3** was synthesized according to the literature.[13] ^{1}H NMR (400 MHz, $CDCl_3$, 300 K) δ = 8.54 (d, J = 8.1 Hz, 6H), 8.45 (d, J = 7.7 Hz, 6H), 8.29 (d, J = 8.1 Hz, 6H), 8.23 (d, J = 7.7 Hz, 6H), 4.10 (d, J = 7.1 Hz, 6H), 2.01–1.95 (m, 3H), 1.35–1.17 (m, 120H), 0.83–0.78 (m, J = 6.8 Hz, 18H); ^{13}C NMR (101 MHz, $CDCl_3$, 300 K) δ = 164.25, 146.46, 137.86, 136.12, 131.65, 130.29, 128.79, 127.39, 127.32, 125.46, 121.59, 121.37, 120.30, 81.31, 44.80, 36.85, 32.11, 32.09, 31.98, 30.29, 29.88, 29.84, 29.55, 29.53, 27.15, 26.77, 22.86, 14.28; HR-MALDI-TOF (*m*/*z*): calcd for $C_{140}H_{171}N_3O_6$: 1990.3173; found, 1990.3172.

Conflicts of interest

There are no conflicts to declare.

Acknowledgements

L. Z. thanks the National Science Foundation of China (NSFC) (21672020) and Beijing Natural Science Foundation (2182049). F. W. thanks the National Natural Science Foundation of China (21975071).

Notes and references

1 (*a*) B. Pei, W. Chan and A. W. M. Lee, Anthracene Capped Isobenzofuran: A Synthon for the Preparations of Iptycenes and Iptycene Quinones, *Org. Lett.*, 2011, **13**, 1774–1777; (*b*) B. Kohl, F. Rominger and M. Mastalerz, Rigid π-Extended Triptycenes via a Hexaketone Precursor, *Org. Lett.*, 2014, **16**, 704–707; (*c*) B. Kohl, F. Rominger and M. Mastalerz, Crystal Structures of a Molecule Designed Not to Pack Tightly, *Chem. – Eur. J.*, 2015, **21**, 17308–17313; (*d*) B. Kohl, F. Rominger and M. Mastalerz, A Pyrene-Fused *N*-Heteroacene with Eleven Rectilinearly Annulated Aromatic Rings, *Angew. Chem., Int. Ed.*, 2015, **54**, 6051–6056; (*e*) N. G. White and M. J. MacLachlan, Soluble Tetraaminotriptycene Precursors, *J. Org. Chem.*, 2015, **80**, 8390–8397; (*f*) D. Reinhard, F. Rominger and M. Mastalerz, Synthesis of Triphenylene-Based Triptycenes via Suzuki–Miyaura Cross-Coupling and Subsequent Scholl Reaction, *J. Org. Chem.*, 2015, **80**, 9342–9348; (*g*) B. Kohl, M. V. Bohnwagner, F. Rominger, H. Wadepohl, A. Dreuw and M. Mastalerz, Attractive Dispersion Interactions Versus Steric Repulsion of *tert*-Butyl groups in the Crystal Packing of a D_{3h}-Symmetric Tris(quinoxalinophenanthrophenazine), *Chem. – Eur. J.*, 2016, **22**, 646–655; (*h*) K. Baumgärtner, A. L. M. Chincha, A. Dreuw, F. Rominger and M. Mastalerz, A Conformationally Stable Contorted Hexabenzoovalene, *Angew. Chem., Int. Ed.*, 2016, **55**, 15594–15598; (*i*) C. Dengiz, S. P. Luppino, G. D. Gutierrez and T. M. Swager, Naphthazarin-Polycyclic Conjugated Hydrocarbons and Iptycenes, *J. Org. Chem.*, 2017, **82**, 7470–7480.

2 (*a*) Y. Kim, J. Bouffard, S. E. Kooi and T. M. Swager, Highly Emissive Conjugated Polymer Excimers, *J. Am. Chem. Soc.*, 2005, **127**, 13726–13731; (*b*) T. M. Long and T. M. Swager, Molecular Design of Free Volume as a Route to Low-K Dielectric Materials, *J. Am. Chem. Soc.*, 2003, **125**, 14113–14119; (*c*) Z. Chen and T. M. Swager, Synthesis and Characterization of Poly-(2,6-triptycene), *Macromolecules*, 2008, **41**, 6880–6885; (*d*) H. Ma, J. Chen, L. Tan, J. Bu, Y. Zhu, B. Tan and C. Zhang, Nitrogen-Rich Triptycene-Based Porous Polymer for Gas Storage and Iodine Enrichment, *ACS Macro Lett.*, 2016, **5**, 1039–1043; (*e*) C. Chen, Novel triptycene-derived

hosts: synthesis and their applications in supramolecular chemistry, *Chem. Commun.*, 2011, **47**, 1674–1688.

3 (*a*) A. Krishna, D. Sabba, H. Li, J. Yin, P. P. Boix, C. Soci, S. G. Mhaisalkar and A. C. Grimsdale, Novel hole transporting materials based on triptycene core for high efficiency mesoscopic perovskite solar cells, *Chem. Sci.*, 2014, **5**, 2702–2709; (*b*) K. Kawasumi, T. Wu, T. Zhu, H. S. Chae, T. V. Voorhis, M. A. Baldo and T. M. Swager, Thermally Activated Delayed Fluorescence Materials Based on Homoconjugation Effect of Donor–Acceptor Triptycenes, *J. Am. Chem. Soc.*, 2015, **137**, 11908–11911; (*c*) X. Liu, Y. Cai, X. Huang, R. Zhang and X. Sun, A perylene diimide electron acceptor with a triptycene core for organic solar cells, *J. Mater. Chem. C*, 2017, **5**, 3188–3194; (*d*) S. R. Peurifoy, J. C. Russell, T. J. Sisto, Y. Yang, X. Roy and C. Nuckolls, Designing Three-Dimensional Architectures for High-Performance Electron Accepting Pseudocapacitors, *J. Am. Chem. Soc.*, 2018, **140**, 10960–10964; (*e*) S. Montanaro, D. G. Congrave, M. K. Etherington and I. A. Wright, Homoconjugation enhances the photophysical and electrochemical properties of a new 3D intramolecular charge transfer iptycene displaying deep blue emission, *J. Mater. Chem. C*, 2019, **7**, 12886–12890.

4 (*a*) Z. Zhu and T. M. Swager, Conjugated Polymer Liquid Crystal Solutions: Control of Conformation and Alignment, *J. Am. Chem. Soc.*, 2002, **124**, 9670–9671; (*b*) C. L. Hilton, C. R. Jamison, H. K. Zane and B. T. King, A Triphenylene-Based Triptycene with Large Free Volume Synthesized by Zirconium-Mediated Biphenylation, *J. Org. Chem.*, 2009, **74**, 405–407; (*c*) P. Kissel, D. J. Murray, W. J. Wulftange, V. J. Catalano and B. T. King, A nanoporous two-dimensional polymer by single- crystal-to-single-crystal photopolymerization, *Nat. Chem.*, 2014, **6**, 774–778; (*d*) R. Bhola, P. Payamyar, D. J. Murray, B. Kumar, A. J. Teator, M. U. Schmidt, S. M. Hammer, A. Saha, J. Sakamoto, A. D. Schlüter and B. T. King, A Two-Dimensional Polymer from the Anthracene Dimer and Triptycene Motifs, *J. Am. Chem. Soc.*, 2013, **135**, 14134–14141; (*e*) D. J. Murray, D. D. Patterson, P. Payamyar, R. Bhola, W. Song, M. Lackinger, A. D. Schlüter and B. T. King, Large Area Synthesis of a Nanoporous Two-Dimensional Polymer at the Air/Water Interface, *J. Am. Chem. Soc.*, 2015, **137**, 3450–3453; (*f*) P. Li, Z. Chen, M. R. Ryder, C. L. Stern, Q. Guo, X. Wang, O. K. Farha and J. F. Stoddart, Assembly of a Porous Supramolecular Polyknot from Rigid Trigonal Prismatic Building Blocks, *J. Am. Chem. Soc.*, 2019, **141**, 12998–13002; (*g*) B. Alameddine, N. Baig, S. Shetty, F. Al-Sagheer and S. Al-Mousawi, Microwave-Assisted [4+2] Diels–Alder Cycloaddition of 1,4-Diethynyl Triptycene with Various Cyclopentadienone Derivatives: Promising Building Blocks for Polymer Networks, *Asian J. Org. Chem.*, 2018, **7**, 378–382.

5 (*a*) E. H. Menke, V. Lami, Y. Vaynzof and M. Mastalerz, π-Extended rigid triptycene-trisaroylenimidazoles as electron acceptors, *Chem. Commun.*, 2016, **52**, 1048–1051; (*b*) E. H. Menke, D. Leibold, A. P. Ullrich, Y. Vaynzof and M. Mastalerz, Planar *versus* triptycenylene end-capped aroyleneimidazoles as electron acceptors in organic photovoltaics, *Org. Chem. Front.*, 2017, **4**, 834–838.

6 D. Meng, H. Fu, B. Fan, J. Zhang, Y. Li, Y. Sun and Z. Wang, Rigid Nonfullerene Acceptors Based on Triptycene–Perylene Dye for Organic Solar Cells, *Chem. – Asian J.*, 2017, **12**, 1286–1290.

7 S. R. Peurifoy, E. Castro, F. Liu, X. Zhu, F. Ng, S. Jockusch, M. L. Steigerwald, L. Echegoyen, C. Nuckolls and T. J. Sisto, Three-Dimensional Graphene Nanostructures, *J. Am. Chem. Soc.*, 2018, **140**, 9341–9345.

8 P. Biegger, S. Stolz, S. N. Intorp, Y. Zhang, J. U. Engelhart, F. Rominger, K. I. Hardcastle, U. Lemmer, X. Qian, M. Hamburger and U. H. F. Bunz, Soluble Diazaiptycenes: Materials for Solution-Processed Organic Electronics, *J. Org. Chem.*, 2015, **80**, 582–589.

9 (*a*) D. Kuck, Three-Dimensional Hydrocarbon Cores Based on Multiply Fused Cyclopentane and Indane Units: Centropolyindanes, *Chem. Rev.*, 2006, **106**, 4885–4925; (*b*) T. M. Swager, Iptycenes in the Design of High Performance Polymers, *Acc. Chem. Res.*, 2008, **41**, 1181–1189; (*c*) B. VanVeller, D. J. Schipper and T. M. Swager, Polycyclic Aromatic Triptycenes: Oxygen Substitution Cyclization Strategies, *J. Am. Chem. Soc.*, 2012, **134**, 7282–7285; (*d*) A. M. Dilmaç, E. Spuling, A. D. Meijere and S. Bräse, Propellanes—From a Chemical Curiosity to "Explosive" Materials and Natural Products, *Angew. Chem., Int. Ed.*, 2017, **56**, 5684–5718; (*e*) T. Ikai, T. Yoshida, K. Shinohara, T. Taniguchi, Y. Wada and T. M. Swager, Triptycene-Based Ladder Polymers with One-Handed Helical Geometry, *J. Am. Chem. Soc.*, 2019, **141**, 4696–4703.

10 B. Hu, C. An, M. Wagner, G. Ivanova, A. Ivanova and M. Baumgarten, Three-Dimensional Pyrene-Fused N-Heteroacenes, *J. Am. Chem. Soc.*, 2019, **141**, 5130–5134.

11 T. Kubo, S. Miyazaki, T. Kodama, M. Aoba, Y. Hirao and H. Kurata, A facile synthesis of trinaphtho[3.3.3]propellane and its π-extension and the formation of a two-dimensional honeycomb molecular assembly, *Chem. Commun.*, 2015, **51**, 3801–3803.

12 T. Kodama, Y. Hirao, T. Nishiuchi and T. Kubo, Elucidation of Intramolecular Through-Space Electronic Communication in aPropeller-Shaped Molecule, *ChemPlusChem*, 2017, **82**, 1006–1009.

13 L. Lv, J. Roberts, C. Xiao, Z. Jia, W. Jiang, G. Zhang, C. Risko and L. Zhang, Triperyleno[3,3,3]propellane triimides: achieving a new generation of quasi-D_{3h} symmetric nanostructures in organic electronics, *Chem. Sci.*, 2019, **10**, 4951–4958.

14 (*a*) C. L. Lee, K. B. Lee and J. J. Kim, Polymer phosphorescent light-emitting devices doped with tris(2-phenylpyridine) iridium as a triplet emitter, *Appl. Phys. Lett.*, 2000, **77**, 2280–2282; (*b*) K. M. Vaeth and C. W. Tang, Light-emitting diodes based on phosphorescent guest/polymeric host systems, *J. Appl. Phys.*, 2002, **92**, 3447–3453.